Perpendicular anisotropy in Ni rich Ni_xMn_{1-x} ultrathin films

2004 J. Phys.: Condens. Matter 16 6029

(http://iopscience.iop.org/0953-8984/16/34/004)

INSTITUTE OF PHYSICS PUBLISHING JOURNAL OF PHYSICS: CONDENSED MATTER

J. Phys.: Condens. Matter **16** (2004) 6029–6040 PII: S0953-8984(04)76617-5

Perpendicular anisotropy in Ni rich Ni_xMn_{1-x} ultrathin films

R Thamankar, S Bhagwat and F O Schumann[1]

Institut für Experimentalphysik, Freie Universität Berlin, Arnimallee 14, 14195 Berlin, Germany

E-mail: schumann@physik.fu-berlin.de

Received 18 February 2004
Published 13 August 2004
Online at stacks.iop.org/JPhysCM/16/6029
doi:10.1088/0953-8984/16/34/004

Abstract

Ni/Cu(100) films are known to exhibit an 'inverse' spin reorientation transition (SRT). The magnetization rotates from in-plane to out-of-plane upon increasing the thickness. The driving force of this phenomenon is a volume uniaxial anisotropy due to the tetragonal film structure, which favours an out-of-plane orientation. We investigated the structure and magnetism of Ni_xMn_{1-x} alloys on Cu(100). We find an improved growth of Ni_xMn_{1-x} alloy films compared to Ni/Cu(100). The SRT of Ni_xMn_{1-x} alloy films is studied using the magneto-optical Kerr effect (MOKE). We find that a Ni-type reorientation can be observed for Mn contents up to 13%. For two concentrations, we were able to determine the volume anisotropy K_V and surface anisotropy K_S values using hard axis magnetization curves, which we discuss in the context of experimentally determined Ni/Cu(100) anisotropy values. We find that the driving force of the reorientation is a positive K_V due to a tetragonal distortion. The positive value of K_V can be related to the magneto-elastic properties although the variation of the reorientation thickness d_c as a function of Mn concentration fails within this model.

1. Introduction

It is well established that Ni/Cu(100) films display a spin reorientation transition (SRT) as a function of thickness. For a coverage up to 7–11 ML the magnetization M is in-plane and for thicker films out-of-plane [1–4]. We found for room temperature grown Ni/Cu(100) films a d_c value of ∼9.5 ML in agreement with previous studies [1–4]. The driving force of the perpendicular orientation is the tetragonal distortion of these films due to pseudomorphic growth on Cu. This leads to a volume anisotropy K_V which is two orders of magnitude larger than the usual cubic anisotropy [3]. Recently the effect of small quantities of Co and Fe on the

[1] Author to whom any correspondence should be addressed.

reorientation transition of Ni films has been studied [5–7]. It was found that d_c increased by a factor of ∼2 when the impurity concentration was ∼6%. We have used a magneto-elastic model (introduced earlier [3]) to explain this behaviour which agrees well with the experimental results [7]. Magnetic random access memory (MRAM) makes use of magnetoresistance effects which occur if the relative orientation of M for two separated magnetic layers is changed [8]. This orientation change is normally achieved via the application of magnetic fields. It is also known that the direction of M can be varied by magnetostriction and piezoelectric methods [9, 10]. Recently Kim *et al* used this concept in a hybrid system containing a ferromagnet and piezoelectric elements [11]. Applying a voltage to the piezo-elements resulted in a strain of the ferromagnet; since their material showed strong magnetostriction it was possible to rotate M from out-of-plane to in-plane. Ni rich Ni_xMn_{1-x} bulk alloys also show strong magnetostriction; therefore we were motivated to study ultrathin Ni_xMn_{1-x}/Cu(100) films. Further, Mn is an interesting 3d element with various magnetic properties. In the bulk, $Ni_{1-x}Mn_x$ alloys show different magnetic properties. Ni rich Ni_xMn_{1-x} alloys display ferromagnetism up to a Mn concentration of ∼22%. In this paper we concentrate on this regime only. The onset of antiferromagnetic order is found at an Mn content of about 30–35%. In between these two regimes, coexisting ferromagnetic long range order and antiferromagnetic short range order are found [12–14]. Thus it is interesting to study how the magnetic properties of ultrathin Ni/Cu(100) films are affected by the addition of Mn. In this paper we discuss the growth, the structure and the SRT of Ni rich $Ni_{1-x}Mn_x$/Cu(100) alloy films.

2. Experimental details

The experiments were performed in an UHV chamber (1×10^{-10} mbar) equipped with a LEED (low electron energy diffraction) optics for structural analysis and CMA (cylindrical mirror analyser) for chemical analysis. A second electron gun for RHEED (reflective high electron diffraction) studies during the growth is also available. Electron beam sources were used for the growing Ni and Mn. The rate of all evaporators can be controlled by individual quartz crystal monitors. These were not located at the sample position but roughly halfway between the sample and evaporation charge. In order to convert the reading into absolute thickness we used RHEED oscillations. Ni grows pseudomorphically on Cu(100) and well separated RHEED oscillations are found [1]. Similarly well documented oscillations exist for Fe/Cu(100) [15]. The calibration of the Mn evaporator is not so straightforward since no RHEED oscillations for Mn/Cu(100) exist. We adopted the following procedure for the calibration of the Mn source. We obtained RHEED oscillations for a $\sim Fe_{50}Mn_{50}$ alloy during the growth on Cu(100) [16, 17]. From this experiment we can determine the total thickness of the alloy film. Since the Fe source is already calibrated we know the amount of Fe deposited. From the difference of the total thickness and the Fe contribution we can calculate the Mn contribution. This gives us the calibration value for the Mn source. Additionally we use Auger spectroscopy to determine the Fe concentration. Since we know the Fe amount we can determine the Mn contribution to yield the concentration measured with Auger spectroscopy, independently confirming the result from the RHEED experiment. At regular intervals the calibration values were checked; we found them to be stable within 5%. A well ordered Cu(100) surface was prepared via Ar^+ ion sputtering and annealing to 720 K. Alloy films were deposited at 300 K by simultaneous deposition at a rate of ∼0.2 ML min^{-1} at a vacuum of 5–7 $\times 10^{-10}$ mbar with the mass spectrometer showing only H_2 as the major peak. At present the lowest temperature that we can achieve is 110 K with LN_2 cooling. For magnetic measurements we utilized the magneto-optical Kerr effect (MOKE); our set-up allows us to perform these experiments at the growth position. The in-plane and out-of-plane magnetization

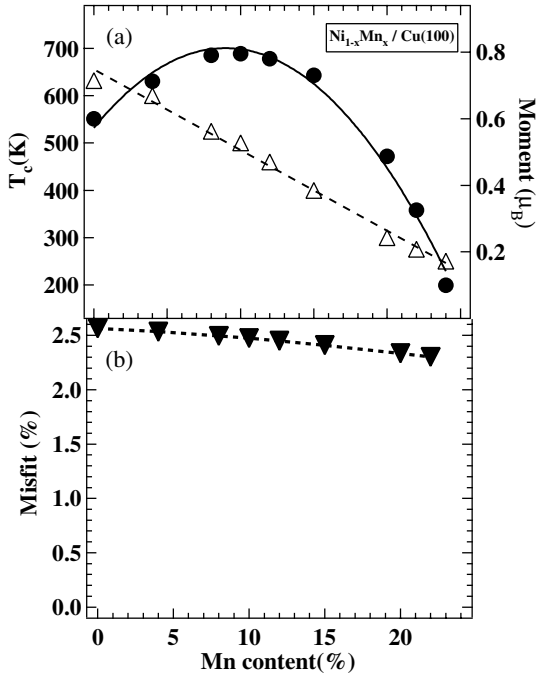

Figure 1. In panel (a) we show the concentration dependence of T_c (△) and the average magnetic moment (●) for bulk fcc Ni_xMn_{1-x} alloys measured at 77 K [18, 19]. In panel (b), the lattice misfit (▼) with respect to Cu(100) is shown using bulk lattice constants [21]. The lines are a guide to the eye.

can be probed by means of orthogonal magnets. Therefore no sample movement is necessary for Kerr measurements along the two directions. The maximum available field is at present ∼1000 G.

3. Growth of Ni_xMn_{1-x} alloy films

We start by reviewing the bulk phase diagram of disordered bulk fcc Ni_xMn_{1-x} alloys. In figure 1(a) we plot on the left (right) axis the Curie temperature T_c (average moment) as a function of the Mn content [18]. We see that T_c decreases almost linearly from 632 K for pure Ni to 250 K for a Mn content of 25%. We note that the average moment of bulk Ni_xMn_{1-x} alloys increases initially, up to 10% of Mn. Then it gradually decreases to almost zero at about 25% Mn [19, 20]. It is found that the lattice constants of the fcc Ni_xMn_{1-x} alloys increase with the Mn content [20, 21]. This results in a misfit for growth on Cu(100), which varies from 2.5 to 2.25% if the Mn content is changed from 0 to 20%; see figure 1(b). Thus it is reasonable to expect pseudomorphic growth as observed for Ni/Cu(100) [3]. The growth of these films is studied by monitoring the RHEED intensity of the specular beam; see figure 2(a). The intensities are normalized such that they can be compared to each other. At the start of the growth, the intensity is 1. Further, the curves are shifted along the y-axis for clarity. The arrow indicates the intensity scale. For Ni we observe clear oscillations which decay with thickness; this is in line with the known start of multilayer growth at ∼6 ML [22, 23]. The behaviour of $Ni_{90}Mn_{10}$ and $Ni_{83}Mn_{17}$ is markedly different since RHEED oscillations persist up to 17 ML. Further, the overall intensity levels are also higher than for Ni growth. For the alloy the intensity

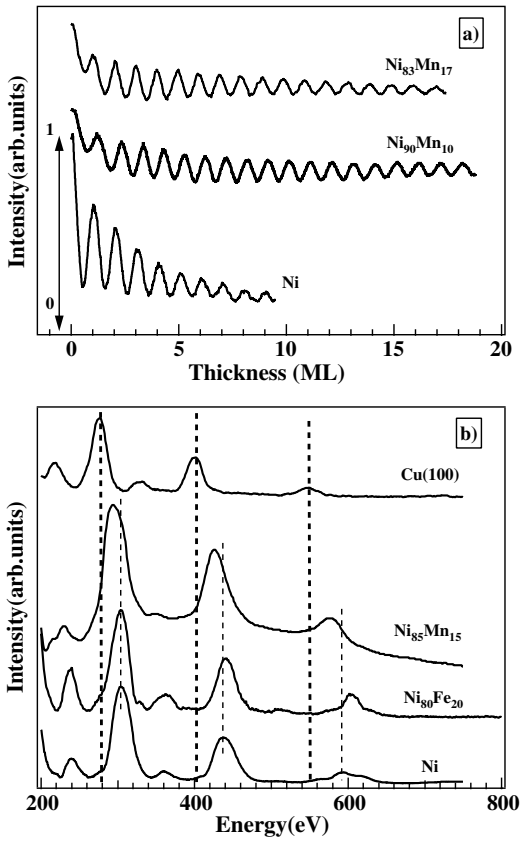

Figure 2. In panel (a) we show the RHEED intensity oscillations of Ni_xMn_{1-x} and Ni films on Cu(100). An extended layer-by-layer growth regime is found. In panel (b) we show the LEED I–V spectra of the (0, 0) beam for Cu(100), 5 ML $Ni_{85}Mn_{15}$, 5 ML $Ni_{80}Fe_{20}$ and 5 ML Ni/Cu(100). The dotted lines through the major Bragg peaks are a guide to the eye. The experiments were performed at 300 K.

at the maxima attains values of ∼0.8. The maximum at the 1 ML position of Ni/Cu(100) has a value of ∼0.5, which for subsequent maxima becomes smaller. We conclude that Ni rich Ni_xMn_{1-x}/Cu(100) films show improved epitaxial growth compared to Ni/Cu(100). This kind of extended layer-by-layer growth mode is similar to that of Ni on pre-oxidized Cu(100) [24].

In order to determine the structure of these alloy films, we employed the LEED I–V curve of the (0, 0) beam. In this way it is possible to obtain the perpendicular lattice constant $d_\perp$ of these films [25]. This will in turn reveal whether the films are tetragonally distorted as we expect from the lattice misfit displayed in figure 1(b). In figure 2(b) we show LEED I–V curves of 5 ML $Ni_{85}Mn_{15}$, $Ni_{80}Fe_{20}$, Ni films and the Cu(100) substrate. Dotted lines through major Bragg peaks are a guide to the eye. It is immediately clear that the major Bragg peaks have shifted to higher energies compared to the Cu(100) substrate case. To determine the perpendicular lattice constants of these alloy films we use a simplified formula given by [25]

$$d_\perp = \frac{n\pi\hbar}{\sin\theta\sqrt{2m_e[E - V_0]}} \tag{1}$$

where E is the energy corresponding to the major peaks, V_0 is the inner potential which has a value of 10 eV. The mass of the electron is given by m_e and n is the order of diffraction. This

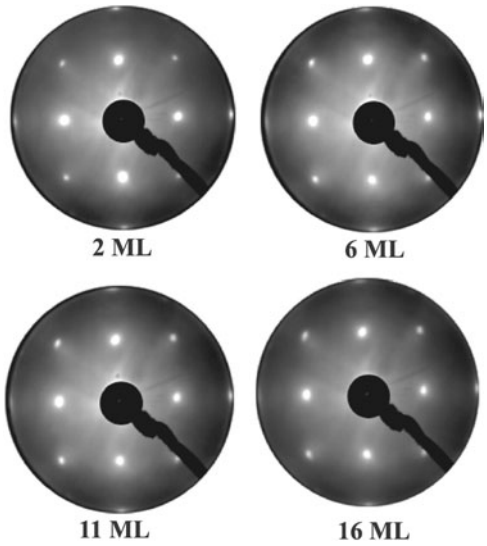

Figure 3. We show LEED images for $Ni_{85}Mn_{15}$ alloy films at different coverages measured at 300 K. The primary electron energy is 140 eV. All the images correspond to a p(1 × 1) symmetry.

Table 1. The perpendicular constants determined using the LEED I–V curves shown in figure 2(b).

System	Thickness	$d_\perp$ (Å)
Cu(100)	—	1.83
Ni	5	1.78
$Ni_{85}Mn_{15}$	5	1.80
$Ni_{80}Fe_{20}$	5	1.74

kind of analysis is sensitive to variations of $d_\perp$ of the order of 0.02 Å [26]. The perpendicular lattice constants determined using the I–V curves are shown in table 1. We find that the variation of the perpendicular lattice constant between Ni and $Ni_{85}Mn_{15}$ amounts to 0.02 Å, which is at the limit of what this simple analysis can do. Consequently we did not try to measure $d_\perp$ for smaller Mn content. The values show that the alloys films a have smaller $d_\perp$, indicating a tetragonal structure assuming pseudomorphic growth.

From the curves shown in figure 2(b), the energy shift for the Ni films is the largest. For 5 ML $Ni_{85}Mn_{15}$ film the shift is smaller. For comparison, we have also displayed the LEED I–V curve for 5 ML $Ni_{80}Fe_{20}$ alloy film also. It is known that Ni film undergoes a tetragonal distortion when grown on Cu(100). This tetragonal distortion introduces a volume anisotropy (which is two orders of magnitude stronger, favouring out-of-plane magnetization [3]. We expect a similar situation for Ni rich Ni_xMn_{1-x} alloy films, which we will discuss below.

The symmetry of the alloy films is p(1 × 1) up to at least 25 ML in the concentration interval 0–15% Mn. Selected LEED patterns of $Ni_{85}Mn_{15}$ films are displayed in figure 3. From the lattice mismatch we would have expected this symmetry. However, a c(2 × 2) superstructure could have been possible if significant Mn surface segregation had taken place, because 0.5 ML on Cu(100) and Ni/Cu(100) display this structure [27–30]. The lack of a c(2 × 2) structure shows that there is no significant surface segregation on Mn. Instead, Auger spectra revealed an enhancement of the Ni Auger peak indicating segregation of Ni.

4. The spin reorientation transition and magneto-elastic contributions

In order to explain the SRT of ultrathin films, the relevant uniaxial anisotropy contributions to the total magnetic energy should be considered. In general the total magnetic anisotropy energy as a function of the film thickness d can be written in first order as

$$K_{\mathrm{eff}} = \frac{2K_{\mathrm{S}}}{d} + K_{\mathrm{V}} - 2\pi M^2. \tag{2}$$

K_{V} and K_{S} refer to the volume and surface anisotropy, whereas the shape anisotropy is given by $2\pi M^2$. For $K_{\mathrm{eff}} > 0$ (<0) the magnetization is out-of-plane (in-plane). In this approximation no continuous change of M is possible; this is only possible if higher order terms are included [31]. One can define two thicknesses where M is either fully out-of-plane or in-plane; the difference gives the interval where M rotates. For Ni/Cu(100) it turns out that these thicknesses are virtually identical [32]. In view of this, we neglect this in the following.

For a SRT to take place K_{eff} must be zero; rearranging equation (2) yields the reorientation thickness d_{c}:

$$d_{\mathrm{c}} = \frac{-2K_{\mathrm{S}}}{K_{\mathrm{V}} - 2\pi M^2}. \tag{3}$$

In general there is a lattice misfit between the substrate and the film. If pseudomorphic growth takes place, the substrate imposes a stress ϵ_1 on the film, resulting in a change of the perpendicular lattice constant. The perpendicular strain ϵ_2 can be calculated using the elastic constants c_{11} and c_{12} [10]:

$$\epsilon_2 = -\frac{2c_{12}}{c_{11}}\epsilon_1. \tag{4}$$

This will result in a distorted structure and taking magnetostriction into account we can derive for K_{V}, where λ_{100} is the magnetostriction constant along the [100] direction [10, 20],

$$K_{\mathrm{V}} = \frac{3}{2}\lambda_{100}(c_{11} - c_{12})(\epsilon_2 - \epsilon_1) = \frac{3}{2}\lambda_{100}\left(\frac{2c_{12}^2}{c_{11}} - c_{11} - c_{12}\right)\epsilon_1. \tag{5}$$

This contribution is two orders of magnitude larger than the cubic anisotropy and, due to its positive sign, the driving force of the SRT of Ni/Cu(100) [3]. For this system the magneto-elastic model yielded the correct value of K_{V} when compared to the experimental data. Since we expect a tetragonal distortion also in $\mathrm{Ni}_x\mathrm{Mn}_{1-x}$, it is appealing to extend this model to this alloy system. According to equation (5) K_{V} is the product of three terms. The first (λ_{100}) is plotted in figure 4(a). We note that λ_{100} varies by more than a factor of 5. Regarding the second term there is some uncertainty, since we are not aware of elastic constants for $\mathrm{Ni}_x\mathrm{Mn}_{1-x}$ alloys in the concentration regime 0–20% Mn. The concentration dependence of ϵ_1 or misfit is displayed in figure 1(b). Using the LEED data shown in table 1 we have evaluated the third term $(\epsilon_2 - \epsilon_1)$ for $\mathrm{Ni}_{85}\mathrm{Mn}_{15}$ which is of the order of -0.016. The value of this difference in the framework of the magneto-elastic model is of the order of -0.055 which is three times the experimentally determined value. In other words the experimentally determined difference is dropping faster than expected in the model. Hence we can conclude that numerically the concentration dependence of K_{V} is governed by λ_{100} and $\epsilon_2 - \epsilon_1$. We have evaluated the concentration dependence of K_{V} and this is shown in figure 4(b). We find that a positive value of K_{V} is possible in our alloy system; hence a Ni-type SRT can be expected for Ni rich alloy films. Since K_{V} depends on the temperature and T_{c} on the Mn content (figure 1(a)) it is useful to include a reduced temperature t $(=T/T_{\mathrm{c}})$ scale in figure 4(b). Additionally we plot anisotropy data for Ni/Cu(100) films from FMR studies at two different reduced temperatures [3, 24, 33]. Also our results (●), to be discussed in the next section, have been

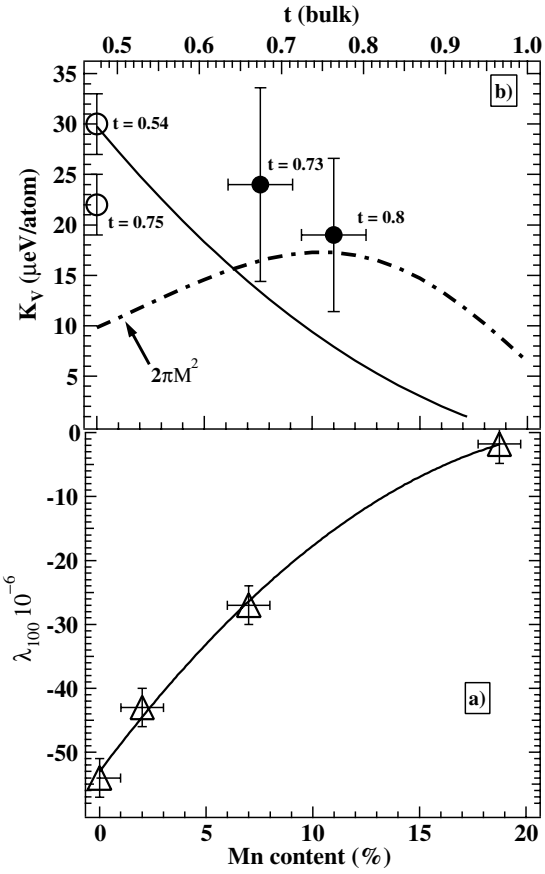

Figure 4. Panel (a) shows the variation of λ_{100} for bulk Ni_xMn_{1-x} alloys [20]; the curve serves as a guide. In panel (b) the evolution of K_V for Ni_xMn_{1-x}/Cu(100) films according to equation (5) is shown. The dashed–dotted curve displays the shape anisotropy. The upper x-axis shows the corresponding reduced temperature t of the bulk alloys at 300 K. Open symbols (○) represent K_V data for Ni/Cu(100) [3, 24, 33]. Closed symbols (●) are experimentally determined values with the corresponding reduced temperatures t; see below.

included. In order to make predictions of d_c according to equation (3) we need input regarding the shape anisotropy and K_S. For the latter we use a constant value of $K_S = -83\ \mu$eV/atom from the latest FMR (ferromagnetic resonance) experiments [24, 33], because K_V is positive only up to 20% Mn. We use (low temperature) bulk values of M as plotted in figure 1, which we corrected for temperatures of 300 K. This will yield 10% reduction of M, when compared to the value at 0 K [9]. This is justified since above 8 ML bulklike behaviour is given [1, 34]. The concentration dependence of $2\pi M^2$ has been included in figure 4(b), too. The crossing point of the $2\pi M^2$ and the K_V curves will cause a rapid increase of d_c as we see if we recall equation (2). Numerically it turns out that this is at 6% Mn. This is shown below in figure 6 together with experimental observations. One may question some of the assumptions made above as follows:

(i) Bulk first-order magneto-elastic coupling constants fail in the description of ultrathin films [35]. For Ni/Cu(100) a recent study showed that the magneto-elastic constants

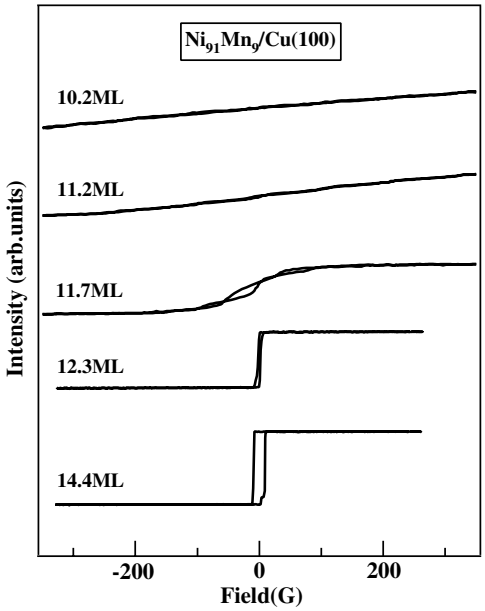

Figure 5. We display the evolution of the out-of-plane magnetization with thickness for a $Ni_{91}Mn_9$ alloy film. The reorientation transition is complete at ∼12 ML. The signal levels are normalized so that they can be directly compared to each other. The loops were obtained at 300 K.

are strain dependent [36]. Consequently using equation (5) may lead to an erroneous determination of K_V.

(ii) Additionally to the fact that enhanced moments at a surface are possible, different orientations of the Mn moment with respect to Fe spins are possible [37]. Applying this to our case we see that we may encounter a decreased average moment.

The purpose of the above discussion is to provide a road map regarding the SRT. Although as mentioned earlier K_V values may have large uncertainties, we can explain a positive K_V as a result of a tetragonal distortion and magnetostriction. We predict this to be limited to the Ni rich side which is confirmed by our magnetic measurements; see below.

5. Magnetic properties

We have studied the magnetic properties of Ni rich Ni_xMn_{1-x} alloy films via the magneto-optic Kerr effect at 300 K. In figure 5 we show selected M–H loops near the SRT for a $Ni_{91}Mn_9$ alloy film. The intensity levels have been normalized; therefore the heights of the loops can be directly compared.

Up to a thickness of 10 ML, we detect in-plane square loops and no perpendicular signal. In other words, the easy axis is in-plane. At about 10.2 ML, we start to detect an out-of-plane signal with no remanence; hence we observe a hard axis loop. Due to the limited fields available, we are not able to achieve saturation. Further thickness increase leads to an intensity increase and at 11.7 ML we are able to achieve saturation. Finally, at 12.3 ML we detect square polar hysteresis loops and the reorientation transition is complete. Compared to that for Ni/Cu(100), the value of d_c has increased by ∼3 ML. We have systematically varied the Mn content and performed similar thickness dependent studies. The result is displayed in

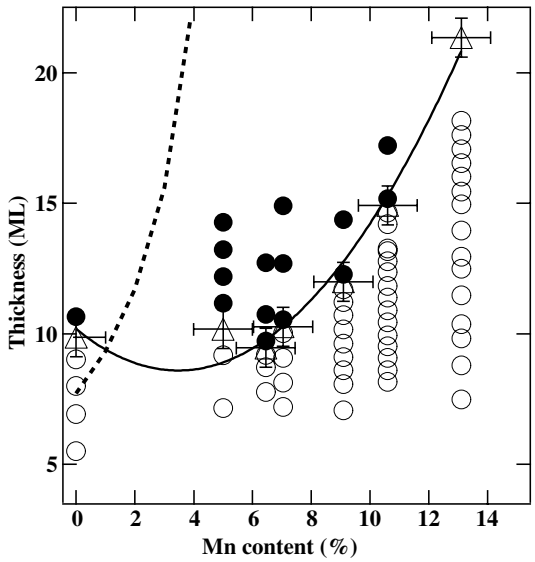

Figure 6. This graph shows the orientation of M (in-plane (○), out-of-plane (●)) as a function of thickness and concentration as determined at 300 K. Also plotted are d_c values (△). The solid curve is a guide to the eye; the dotted curve results from a magneto-elastic model. See the text.

figure 6. The error bars for d_c are due to the error in determination of the exact thickness, which we determined in the following way. We linearly extrapolated the out-of-plane saturation signal towards the reorientation regime and we looked at the thickness where the remanence equals 50% of the extrapolated signal. Our experiments show that increasing the Mn content shifts d_c shifts towards higher values. For 13% Mn the value of d_c has increased by 100% as compared to that for Ni/Cu(100). This behaviour can be readily understood if we recall equation (3). Mathematically speaking, d_c has a pole were the value of K_V is matched by the shape anisotropy. A similar rapid increase of d_c is observed for $Co_{1-x}Ni_x$, $Fe_{1-x}Ni_x$ and N_xPd_{1-x} alloy films [5, 6, 38, 7, 39].

Increase of the Mn content beyond 13% results in in-plane loops for all thicknesses. In figure 6 we have included the result for d_c (dashed curve) derived from equation (3). It is obvious that the magneto-elastic model describes the experimental data only qualitatively, but the position of the pole is significantly shifted, by ∼6%, from the experimental value of ∼13%. Potential reasons for the discrepancy between experimental and predicted values of d_c have been discussed above.

During the course of these experiments we were able to obtain hard axis loops over an extended thickness regime for concentrations near the pole of d_c. As an example we show polar loops for a $Ni_{87}Mn_{13}$ sample; see figure 7(a). At 12.8 ML we are able to achieve saturation when the applied field exceeds ∼550 G. The inset in figure 7(b) shows the definition of the saturation field H_s. Since the actual loops show some rounding when approaching saturation we have employed the following procedure to determine H_s. In the regime where M varies linearly we can fit a linear curve, which we can extrapolate to high fields. At high fields M is constant; this curve can be extrapolated towards smaller fields. The intercept of these two curves yields the value of H_s. We observe that further thickness increase leads to a rapid decrease of the field H_s. It is now appealing to plot H_s versus the inverse thickness; the result is shown in figure 7(b). It becomes apparent that a linear curve describes the situation very

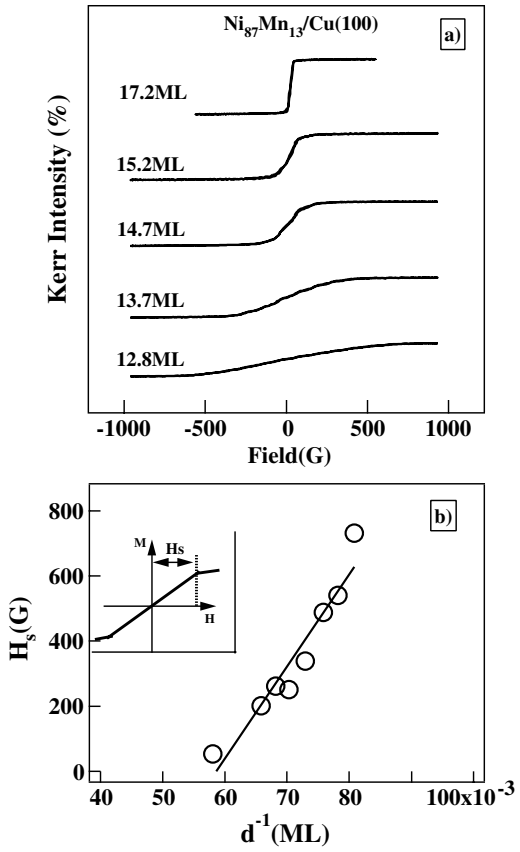

Figure 7. Panel (a) shows set of hard axis polar M–H loops taken for a $Ni_{87}Mn_{13}$ sample at 300 K. In panel (b) we plot the saturation field (H_s) versus the inverse thickness d^{-1}; a linear curve describes the experimental data well. The inset in panel (b) explains the definition of H_s.

well. Similar plots for the anisotropy are being employed in order to derive the contributions of the surface/interface and volume, respectively.

It is well known that in the case of a uniaxial anisotropy K_{eff} the following relation for a hard axis loop holds:

$$H_s = \frac{2(-K_{\text{eff}})}{M} = -2\frac{2K_s/d + K_V - 2\pi M^2}{M}. \tag{6}$$

In other words there exists a proportionality between H_s and $-K_{\text{eff}}$. The minus sign is due to the fact that an in-plane easy axis (out-of-plane hard axis) means a negative K_{eff} in our notation. It follows immediately from figure 7(b) that the linear curve has a positive slope and a negative y-axis intercept. Therefore $K_V - 2\pi M^2$ is positive and K_s is negative, without resorting to a further analysis. In other words, the driving force of the SRT in Ni_xMn_{1-x} alloys is a positive K_V. Recalling equation (2) it is therefore straightforward to determine K_S and K_V from the H_s versus d^{-1} plot, although it would be desirable to determine absolute values of anisotropy constants via dedicated techniques such as FMR investigation. Taking into account shape anisotropy via bulk magnetization data as explained above, we found for K_V 24 and 19 μeV/atom for 9 and 13% Mn, respectively. These data have been included in figure 4(b) as closed symbols (●). The error bars include the error in the value considered

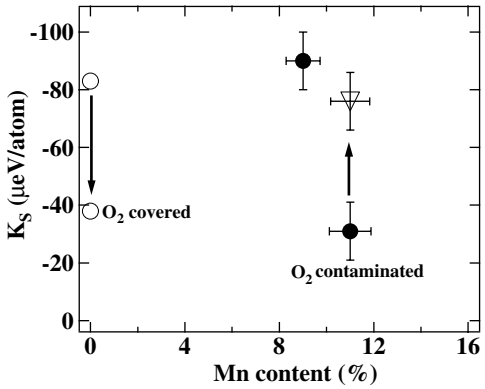

Figure 8. This figure shows experimentally determined K_S (●) values for $Ni_{92}Mn_8$ and $Ni_{89}Mn_{11}$ alloys. Open symbols (○) relate to available data on Ni films grown on clean and pre-oxidized Cu(100) [24].

for M and the error in determining H_s. The important point that is seen from the figure is that K_V is positive. A positive K_V arises from the magnetostriction since we observe a tetragonal distortion for the alloy films. Additionally, we determined the reduced temperature t for the samples with 9 and 11% Mn. We are not aware of any study regarding the $T_c(d)$ behaviour of Ni_xMn_{1-x} alloy films. From the $T_c(d)$ behaviour of Ni films, we know that at about 15 ML, the T_c would reach 80% of the bulk value [1, 40]. From figure 1(a) we find that for a $Ni_{91}Mn_9$ sample, the bulk T_c is ∼520 K. Thus at a thickness of 15 ML, T_C would be ∼420 K. This implies that our measuring temperature of 300 K corresponds to $t \sim 0.73$ in reduced temperature units. A similar calculation for a $Ni_{89}Mn_{11}$ sample yields $t \sim 0.8$. Similarly we obtained the corresponding K_S values as shown in the figure 8. We determined K_S as -90 and -31 μeV/atom for $Ni_{91}Mn_9$ and $Ni_{87}Mn_{17}$, respectively. Even though there is a scatter in the values determined, K_S favours in-plane magnetization, which is consistent with the requirements for a Ni-type SRT to occur; see the previous section. The K_s of $Ni_{89}Mn_{11}$ deviates strongly compared to the case for the clean Ni and $Ni_{91}Mn_9$ samples. An Auger scan at the end of this experiment revealed oxygen contamination. For Ni/Cu(100), oxygen contamination gives a decreased negative value of K_S [24, 33]. Similarly, the drastic change could be attributed to the contamination of the film. Finally, we would like to point out that the observation of a Ni-type SRT implies that the films must grow pseudomorphically on Cu(100) resulting in a tetragonal structure. Only this ensures that a strong volume anisotropy exists, which favours an out-of-plane magnetization.

6. Summary

We have investigated Ni rich Ni_xMn_{1-x} alloy films grown on Cu(100) and determined structural and magnetic properties. We find that these films show an improved layer-by-layer growth compared to Ni/Cu(100). Further, these films display a p(1 × 1) LEED pattern and are tetragonally distorted due to the lattice mismatch to the Cu substrate. These films exhibit a reorientation transition analogous to that of Ni/Cu(100). We find that the critical thickness d_c is concentration dependent and is almost doubled at 13% Mn compared Ni/Cu(100). Above this Mn content we observe only an in-plane orientation of M. For two concentrations we are able to derive anisotropy constants via hard axis loops. They confirm that a positive K_V is the driving force for a perpendicular orientation of M. A magneto-elastic model

explains the appearance of the positive K_V, but fails to describe the reorientation thickness quantitatively.

Acknowledgment

This work was supported by the Deutsche Forschungsgemeinschaft via SFB 290 (TP A11).

References

[1] Huang F, Kief M T, Mankey G J and Willis R F 1994 *Phys. Rev.* B **49** 3962
[2] Jungblut R, Johnson M T, aan de Stegge J, Reinders A and den Broeder F J A 1994 *J. Appl. Phys.* **75** 6424
[3] Schulz B and Baberschke K 1994 *Phys. Rev.* B **50** 13467
[4] Vollmer R, Gutjahr-Löser T, Kirschner J, van Dijken S and Poelsema B 1999 *Phys. Rev.* B **60** 6277
[5] Lin M T, Lin W C, Kuo C C and Chiu C L 2000 *Phys. Rev.* B **62** 14268
[6] Lin W C, Kuo C C, Chiu C L and Lin M-T 2001 *Surf. Sci.* **478** 9
[7] Thamankar R, Ostroukhova A and Schumann F O 2002 *Phys. Rev.* B **66** 134414
[8] Parkin S S P, Roche K P, Samant M G, Rice P M, Beyers R B, Scheuerlein R E, O'Sullivan E J, Brown S L, Bucchigano J, Abraham D W, Lu Y, Rooks M, Trouilloud P L and Wanner R A 1999 *J. Appl. Phys.* **85** 5828
[9] Kittel C 1991 *Introduction to Solid State Physics* (New York: Wiley)
[10] Chikazumi S 1964 *Physics of Magnetism* (New York: Wiley)
[11] Kim S-K, Lee J-W, Shin S-C, Song H W, Lee C H and No K 2003 *J. Magn. Magn. Mater.* **267** 127
[12] Cable J W and Tsunoda Y 1994 *Phys. Rev.* B **50** 9200
[13] Abdul-Razzaq W and Kouvel J S 1987 *Phys. Rev.* B **35** 1764
[14] Abdul-Razzaq W and Kouvel J S 1984 *J. Appl. Phys.* **55** 1623
[15] Thomassen J, May F, Feldmann B, Wuttig M and Ibach H 1992 *Phys. Rev. Lett.* **69** 3831
[16] Thamankar R, Bhagwat S and Schumann F O 2004 *Phys. Rev.* B **69** 054411
[17] Offi F, Kuch W and Kirschner J 2002 *Phys. Rev.* B **66** 064419
[18] Wassermann E F 1990 Invar: moment–volume instabilities in transition metals and alloys *Ferromagnetic Materials* ed K H J Buschow and E P Wohlfarth (Amsterdam: North-Holland) pp 238–322
[19] Tange H, Tokunaga T and Goto M 1978 *J. Phys. Soc. Japan* **45** 105
[20] Stearns M B 1986 *Properties of Magnetic Materials* (*Landolt–Börnstein*) ed H P J Wijn (Berlin: Springer)
[21] Pearson W B 1964 *A Handbook of Lattice Spacings and Structures of Metals and Alloys* (Oxford: Pergamon)
[22] Shen J, Giergil J and Kirschner J 1995 *Phys. Rev.* B **52** 8454
[23] Poulopoulos P, Lindner J, Farle M and Baberschke K 1999 *Surf. Sci.* **437** 277
[24] Lindner J, Poulopoulos P, Nünthel R, Kosubek E, Wende H and Baberschke K 2003 *Surf. Sci.* **523** L65
[25] Pendry J B 1974 *Low Energy Electron Diffraction* (London: Academic)
[26] Heinz K 2002 private communication
[27] Wuttig M, Gauthier Y and Blügel S 1993 *Phys. Rev. Lett.* **70** 3619
[28] O'Brien W L, Zhang J and Tonner B P 1993 *J. Phys.: Condens. Matter* **5** L515
[29] O'Brien W L and Tonner B P 1995 *Phys. Rev.* B **51** 617
[30] Schmitz D, Rader O, Carbone C and Eberhardt W 1996 *Phys. Rev.* B **54** 15352
[31] Fritzsche H, Kohlhepp J, Elmers H J and Gradmann U 1994 *Phys. Rev.* B **49** 15665
[32] Farle M, Mirwald-Schulz B, Anisimov A N, Platow W and Baberschke K 1997 *Phys. Rev.* B **55** 3708
Farle M 1998 *Rep. Prog. Phys.* **61** 755
[33] Lindner J 2003 *PhD Thesis* Department of Physics, Freie Unversität, Berlin
[34] Li Y and Baberschke K 1992 *Phys. Rev. Lett.* **68** 1208
[35] Koch R, Weber M, Thürmer K and Rieder K H 1996 *J. Magn. Magn. Mater.* **159** L11
[36] Gutjahr-Löser T, Sander D and Kirschner J 2000 *J. Appl. Phys.* **87** 5920
[37] Rader O, Pampuch C, Gudat W, Dallmeyer A, Carbone C and Eberhardt W 1999 *Europhys. Lett.* **46** 231
[38] Kuo C C, Chuang S F, Pan W, Lin W C and Lin M-T 2002 *J. Appl. Phys.* **91** 7185
[39] Seider M, Kaltofen R, Muschiol U, Lin M-T and Schneider C M 2000 *J. Appl. Phys.* **87** 5762
[40] Schumann F O, Wu S Z, Mankey G J and Willis R F 1997 *Phys. Rev.* B **56** 2668